

# PHOENICS SIMULATIONS OF GAS-LIQUID FLOWS IN LARGE PIPING COMPONENTS RELATED TO NUCLEAR SAFETY ASSESSMENT

M. An and W. Thompson  
Atlantic Nuclear Services Ltd.  
Fredericton, NB, Canada  
[man@ansl.ca](mailto:man@ansl.ca) or [wthompson@ansl.ca](mailto:wthompson@ansl.ca)

M. Wright  
Wright Analytic  
Darlings Island, NB, Canada

V. Agranat  
ACFDA  
Thornhill, ON, Canada  
[vladimir.agranat@utoronto.ca](mailto:vladimir.agranat@utoronto.ca)

M. Kawaji  
University of Toronto  
Toronto, ON, Canada  
[kawaji@ecf.toronto.edu](mailto:kawaji@ecf.toronto.edu)

A.M.C. Chan  
Kinectrics (formerly  
Ontario Power Technologies)  
Toronto, ON, Canada

## ABSTRACT

Two applications of the PHOENICS two-fluid model to analyze gas-liquid flows in large piping components are reported, both of which are related to nuclear safety assessments. The first application includes a series of steady-state simulations of gas-liquid flows in large vertical pipes, in order to validate the code for providing design-stage information on safety sensitive void fraction and flow distribution within the chimney of a simplified boiling water reactor under development, which utilizes natural circulation. The second application is a transient two-phase simulation of an outlet header during a thermosiphoning test performed at a large-scale test facility for existing nuclear reactors. The intent of this simulation was to understand the underlying phenomena that led to certain unexpected behavior during the test, and to determine whether such behavior could possibly occur in an actual full size facility.

## NOMENCLATURE

C = constitutive coefficient  
D = internal pipe diameter  
 $D_b$  = bubble diameter  
F = interfacial force per unit volume  
 $F_{L,r}$  = lateral component of interfacial lift force

G = phase mass flux  
H = enthalpy  
J = superficial velocity  
L = pipe length  
Re = Reynolds number  
r = radial coordinate  
S = source rate  
T = temperature  
t = time  
U = velocity component  
 $\vec{V}$  = velocity vector  
X, Y, Z = coordinate directions  
z = axial coordinate

Greek  
 $\alpha$  = phase volume fraction  
 $\Gamma$  = exchange coefficient  
 $\phi$  = conserved property (dependent variable)  
 $\nu$  = kinematic viscosity  
 $\rho$  = density

Subscripts  
b = bubble  
D = drag force  
g = gas phase  
i = phase index,

inlet	= inlet conditions
j	= velocity component index, $j=1,2,3$
L	= lift force
Low	= small positive number
l	= liquid phase
p	= pressure
r	= relative velocity or lateral component
vm	= virtual mass force
$\phi$	= conserved property
$\mu$	= shear induced turbulence
$\mu_b$	= bubble induced turbulence

## INTRODUCTION

Designers and regulators of commercial nuclear power installations often use test facilities to assess the expected safety performance of such installations. In many thermalhydraulic safety applications, one-dimensional computer programs are used to help in the understanding of such tests, since such programs are generally sufficiently precise. However, when complicated thermalhydraulic features are involved, for example, in large volumes, or complex geometry, particularly with two-phase flows, it is necessary to invoke more fundamentally based 3D CFD codes such as PHOENICS (CHAM 1999a). This paper includes two recent PHOENICS applications for gas-liquid flow analyses where the large piping components involved lead to possible nuclear safety concerns, i.e., gas-liquid flows in a large diameter vertical pipe and in a horizontal header.

The first case relates to steady-state gas-liquid flows in large vertical pipes of test facilities, which can be used to assist in the design of a Simplified Boiling Water Reactor (SBWR). This type of next generation reactor emphasizes the elimination of active safety systems and introduction of passive components in order to improve reliability and safety (Hasanein et al 1996). In an SBWR, natural circulation is adopted for core cooling and the total core flow depends on the net driving head between the downcomer and the chimney. The void fraction and flow distribution in the chimney thus play an important role in providing the desired core flow rate, which can be better understood during the design stage via CFD modeling, which is more economical than prototypical testing.

The second case is a transient two-phase simulation of an outlet header during a thermosyphoning test

performed at a large-scale test facility for existing nuclear reactors. The purpose of the study is to better understand the underlying phenomena that led to certain unexpected behavior during the test, and to determine whether such behavior could possibly occur in an actual full size facility.

In both cases, a two-fluid Eulerian-Eulerian technique, which treats the liquid and gas phases as "inter-penetrating continua" (Lahey et al 1993, Podowski 1997, Alajbegovic et al 1996, CHAM 1999b), was used to solve for the two-phase flow field. This model was coupled with an IPSA (Inter-Phase Slip Algorithm) to determine the inter-phase transfers.

PHOENICS implemented with the above methodology has been extensively validated for two-phase flows in small vertical pipes (see CHAM 1999a and Lahey et al 1993 for more details). However, due to the lack of relevant measurements, it has not been sufficiently validated to provide accurate assessment of the multi-dimensional behavior of two-phase flows in large piping components. In the first case of this paper, two PHOENICS code validations (Agranat et al 1996 and 1998), using the recent experimental data available for gas-liquid up-flows in large diameter vertical pipes (Hasanein et al 1996, Ohnuki et al 1997 and 1996), are reviewed. In the second case, the PHOENICS model was first validated against limited relevant experimental data before it was employed to simulate the transient two-phase flows in a horizontal header.

Therefore, the objective of this paper is to demonstrate the prospect of the two-fluid CFD modeling for analysis of both steady-state and transient gas-liquid flows in large piping components related, in particular, to nuclear safety assessments. The prospect will in turn necessitate the need for more measured data on gas-liquid flows and phase distribution in the large components with different orientations.

## GOVERNING EQUATIONS

As mentioned before, the Eulerian-Eulerian two-fluid model, coupled with the IPSA for inter-phase transfers, was used in both cases. The time-averaged governing conservation equations of within-phase mass, momentum, and energy transports for each phase have the following general form in PHOENICS:

$$\frac{\partial(\alpha_i \rho_i \phi_i)}{\partial t} + \nabla \cdot (\alpha_i \rho_i \vec{V}_i \phi_i - \alpha_i \Gamma_{\phi,i} \nabla \phi_i) = \alpha_i S_{\phi,i} \quad (1)$$

where subscript  $i = l$  or  $g$  for the liquid and gas phases, respectively. In Equation (1),  $t$  stands for time,  $\alpha$  is the volume fraction,  $\rho$  is the density,  $\phi$  is any conserved property,  $\vec{V}$  is the velocity vector,  $\Gamma_{\phi}$  is the exchange coefficient of the entity  $\phi$ , and  $S_{\phi}$  is the source rate of  $\phi$  including those due to inter-phase transfers. The relevant dependent variables for  $\phi$  can be taken as 1 (for continuity), velocity components  $U_{j,i}$  where  $j = 1, 2, 3$ , enthalpy  $H_i$ , or other scalar variables of phase  $i$ .

For simulation of two-phase flow in a vertical pipe, the  $k$ - $\epsilon$  two-equation turbulence model considering bubble-induced turbulence was used to calculate the turbulent viscosity, which, together with the laminar viscosity, contributes to the effective exchange coefficient  $\Gamma_{\phi}$ . For simulation of the horizontal header, however, an algebraic turbulence model, LEVEL (CHAM 1999b), was used, which is especially efficient for flow fields with clustered solid obstacles or complicated wall presence such as that due to inclined small pipes connected to a header (see case 2 below). In this situation, meaningful near wall grids cannot be defined for a more advanced turbulence model.

The inter-phase mass and energy transfers were not considered for either case. For the unsteady simulation of the insulated header, the sole cause for such transfers between steam and liquid water is pressure. Since pressure varies only slightly over the simulation time, the resultant inter-phase mass and energy transfers can be reasonably neglected, thus there is no need to solve the energy equation. The benefit of this simplification is a significantly enhanced convergence for the entire transient header simulation, which is a high priority considering the complexity of the geometry and the nature of two-phase flow within it, as well as the length of the simulation time, as discussed later. The inter-phase momentum sources include those due to interfacial drag, lift, pressure, virtual mass forces etc., which will be detailed later together with relevant applications.

## CASE 1: GAS-LIQUID FLOWS IN LARGE DIAMETER VERTICAL PIPES

### DETAILS OF THE MODEL

The fast parabolic option of the PHOENICS code was first employed to solve the 3D governing equations as the flow considered is a fully developed flow without any recirculation patterns. The following boundary conditions were used: the inlet values of superficial liquid and gas velocities,  $J_l$  and  $J_g$ , are specified and the inlet phase velocities are assumed to be equal, the symmetry condition is applied at the pipe centerline, and the no-slip condition is used at the pipe wall. The calculations for the air-water flows reported here were repeated recently with the elliptic PHOENICS-3.3 solver, and the computational results newly obtained were compared with the experimental data by Ohnuki et al (1997, 1996).

The interfacial drag force,  $\mathbf{F}_D$ , between liquid and bubbles is introduced as the force acting on isolated spherical particles (CHAM 1999b, Lahey et al 1993, Podowski 1997, Alajbegovic 1996). The particle number-density (as a function of the gas volume fraction,  $\alpha_g$ , and the bubble diameter,  $D_b$ ) is  $6\alpha_g/(\pi D_b^3)$ , and hence the total drag force per unit volume, acting on the dispersed phase, is

$$\mathbf{F}_D = -0.75 C_D/D_b \rho_l \alpha_g |\mathbf{V}_r| \mathbf{V}_r \quad (2)$$

where  $\rho_l$  is the liquid phase density, and  $\mathbf{V}_r = \mathbf{V}_g - \mathbf{V}_l$  is the relative velocity vector.

In this study, the interfacial drag coefficient was taken to be the 'dirty water' model (CHAM 1999b):

$$C_D = 6.3/Re_b^{0.385}, \quad Re_b = D_b |\mathbf{V}_r|/\nu_l \quad (3)$$

The interfacial lift force,  $\mathbf{F}_L$ , acting on the dispersed phase and induced by a velocity gradient of the continuous phase in the lateral direction, is defined in Lahey et al (1993). For the pipe flows considered, the vector  $\mathbf{F}_L$  practically reduces to its lateral component:

$$F_{L,r} = -C_L \rho_l \alpha_g V_{r,z} dV_{l,z}/dr \quad (4)$$

where  $V_{r,z} = V_{g,z} - V_{l,z}$  is the axial component of the relative velocity (in  $z$  direction), and  $r$  is the radial distance from the pipe centerline.

There is a significant uncertainty in the value of lift force coefficient,  $C_L$ . Various constant values of  $C_L$  from 0.01 (highly viscous flows) to 0.5 (inviscid flows) are used in the literature. In this modeling, the value of 0.1,

recommended by Lahey et al (1993), was applied in the base cases.

Other interfacial forces (pressure, virtual mass, etc.), acting on the bubbles in the gas-liquid two-phase flows, are not detailed here. They are explained in the literature (CHAM 1999b, Lahey et al 1993, Podowski 1997, Alajbegovic 1996), where the two-phase turbulence models, accounting for the bubble-induced turbulence, can also be found.

## RESULTS AND DISCUSSION

### A. Modeling of a Steam-Water Bubbly Up-Flow in a Large Vertical Pipe

In this section, the numerical results (Agranat et al 1996), obtained for a steam-water up-flow in a large vertical pipe at elevated pressures (up to 7.5 MPa), are briefly reviewed.

The void distributions measured in a 24-inch (50.8cm inner diameter) vertical pipe with steam/water flowing at 230°C or 280°C (Hasanein et al 1996) have been predicted. Calculations were performed in both two dimensions ( $r, z$ ) and three dimensions ( $r, \theta, z$ ), for steady state conditions. The local void fraction, phasic velocities and pressure were predicted for several test conditions. The inlet gas and liquid velocities were estimated from the total mass flux and measured void fraction data using a homogeneous flow model. The solution domain ranged from the exit of the flow straightener to the measurement station 4.2 m downstream (Hasanein et al 1996, Agranat et al 1996).

Three cases with inlet void fractions of  $\alpha_{g,inlet} = 0.205$ , 0.43 and 0.59 at 280°C and three cases with inlet voids of 0.106, 0.205 and 0.46 at 230°C have been simulated. In Table 1, the inlet void fraction,  $\alpha_{g,inlet}$ , and the liquid and gas mass fluxes,  $G_l$  and  $G_g$ , at the inlet are given as well as the measured and calculated pipe-average void fractions. The standard calculations were performed with the bubble diameter,  $D_b$ , set equal to 3 mm.

In all cases, the pipe-average void fraction predicted was in good agreement with the measurements. The radial void fraction distribution was predicted to be almost flat across the pipe diameter (in agreement with the measured data), except for the region near the pipe wall. In the latter, the predicted void fraction increased slightly or

significantly depending on the interfacial force model used. The void fraction profiles computed using the simplified model of PHOENICS 2.0, where only the interfacial drag force is taken into account, showed that the gas phase does not migrate significantly toward the wall region and does not cause the void peaking near the wall. However, for the calculations with the more advanced model of PHOENICS 2.1.3, which accounts not only for the drag force but also for the interfacial lift, pressure and virtual mass forces, the positive radial steam velocities are typical. They lead to a steam flow from the central part of the pipe towards the pipe wall and ultimately to the wall void peaking. The measurements in the OPT's experiments (Agranat et al 1996) did not cover in sufficient detail the pipe wall region, where the above effect is possible. Therefore, more validation of the advanced two-fluid model predictions described is necessary (in the near wall regions).

Table 1: Simulation Conditions and Results (Agranat et al 1996)

Run No.	T (°C)	$G_l$ (kg/m <sup>2</sup> s)	$G_g$ (kg/m <sup>2</sup> s)	$\alpha_{g,inlet}$	$\bar{\alpha}_g$ (Measured)	$\bar{\alpha}_g$ (Calculated)
1	280	2107	24.1	0.205	0.211	0.195
2	280	1652	55.1	0.430	0.409	0.420
3	280	1239	79.3	0.590	0.593	0.583
4	230	1445	2.9	0.106	0.105	0.094
5	230	1119	4.9	0.205	0.206	0.182
6	230	836	12.2	0.460	0.465	0.436

### B. Modeling of Air-Water Bubbly Up-Flows in Large Vertical Pipes

The PHOENICS code was validated for bubbly air-water flows in small vertical pipes, having inner diameters of about 4 to 6 cm, in various papers, e.g., in Lahey et al (1993). However, it was not tested as extensively for gas-liquid flows in larger pipes. The study by Agranat et al (1998) was performed to investigate the capability of the PHOENICS two-fluid model to predict the effects of interfacial lift force and bubble diameter on the lateral gas phase distribution in a turbulent bubbly air-water up-flow in a large diameter vertical pipe (the internal pipe diameter,  $D = 0.2$  m). Parabolic solver of PHOENICS 2.2.1 was first used for the simulation.

The flow parameters investigated in detail in Agranat et al (1998) were as follows:  $D = 0.2$  m,  $L/D = 60$ ,  $J_1 = 1.06$  m/s,  $J_g = 0.033, 0.11, \text{ and } 0.26$  m/s, where  $L$  is the

pipe length,  $J_l$  and  $J_g$  are the superficial velocities of liquid and gas, respectively. The following values of the constitutive coefficients recommended in Lahey et al (1993) were used in the base case:  $C_{vm} = 0.0$ ,  $C_p = 1.0$ ,  $C_L = 0.1$ ,  $C_\mu = 0.09$ ,  $C_{\mu b} = 1.2$  standing for the coefficients of virtual mass, pressure and lift forces respectively, and the shear induced turbulence and the bubble induced turbulence coefficients. The grid employed in the computations consisted of 20x120 cells in the radial and axial directions, respectively. For the present paper, the elliptic solver of PHOENICS 3.3 was applied to simulate the same flow. Figures 1 to 4 show the main computational results obtained, which were evaluated and compared with the gas phase distribution data in Ohnuki et al (1997, 1996).

Figure 1 shows the lateral gas phase distribution calculated under the bubbly flow conditions ( $J_g = 0.033$  m/s), and the experimental data by Ohnuki et al (1997). It is seen that the agreement between the simulation and experimental results is good. The effect of the bubble diameter is also shown. The difference between the phase distributions predicted for  $D_b = 1$  and 2 mm is significant particularly near the pipe wall ( $r = 0.1$  m). For the higher  $D_b$ , the predicted wall void peaking is more pronounced than for the lower  $D_b$ . It can be partially explained by a greater effect of the interfacial lift force on the void distribution in the near-wall region. The lateral void profile predicted for  $D_b = 1$  mm agrees with the experimental distribution better than that for  $D_b = 2$  mm.

Figure 2 shows the lateral gas distribution under higher void fraction conditions ( $J_g = 0.11$  m/s). There is a good agreement between the computational results and the measurement in the pipe core, however, the difference between them near the pipe wall ( $r = 0.1$  m) is larger than that shown in Figure 1 in the case of the lower void fraction ( $J_g = 0.033$  m/s). The same values of the empirical constitutive coefficients are used in both cases ( $J_g = 0.033$  m/s and 0.11 m/s).

Figure 3 shows the computational results under churn bubbly flow conditions where  $J_g = 0.26$  m/s. In this case, the qualitative and quantitative agreement with the experimental gas phase distribution is seen only for a negative value of the lift force coefficient ( $C_L = -0.2$ ). This result shows that the conventional interfacial lift force model with a positive lift force coefficient,  $C_L$ , proposed by Lahey et al (1993), Podowski (1997) and Alajbegovic et al (1996), is not capable of predicting the void core peaking phenomenon in the churn bubbly

air/water up-flow considered in Ohnuki et al (1997). Only negative values of  $C_L$  allow achieving it. A similar result was obtained by Ohnuki et al (1997, 1996) with the ACE-3D code. Thus, further development of the interfacial lift force model is needed to extend the two-fluid model applications to the churn bubbly flow conditions where the coalescence of large bubbles and the core void peaking are observed by Podowski (1997) and Ohnuki et al (1997). Under such conditions, where large bubbles can deform from a spherical shape, the advanced interfacial drag and lift force models for deformed bubbles might be useful.

Figure 4 shows that the effect of the interfacial pressure force on the lateral void distribution is not significant. Indeed, the computational results obtained with and without accounting for the interfacial pressure force ( $C_p = 1.0$  and 0.0) are very close. It should be mentioned that  $C_L$  is equal to 0.1 in this case.

## CASE 2: UNSTEADY STEAM-WATER FLOW IN A HORIZONTAL HEADER

### BACKGROUND

The work described here relates to a two-phase large-scale pressurized test facility. In this facility, five electrically heated horizontal sections, denoted as HS10 to HS14 respectively for later reference, are connected to inlet and outlet headers via inlet and outlet feeders. In normal (pumped) circulation mode, heat is removed from the coolant after the outlet header, and then the cooled liquid is pumped back to the inlet header. During a test in this rig at an initial pressure of 7MPa, in which the normally operating circulating pump was "tripped", the acceptable heat removal via thermosyphoning flow patterns did not remain established. The normal flow direction of the coolant in two of the five heated channels, i.e. in HS12 then HS11, reversed, after which flow stalled entirely in HS11. This was followed by heat up of this channel. Initial loop analyses of the test with a 1D code indicated that the outlet header might have played a significant part in these observations.

### SCOPE OF THE WORK

The transient 3D two-phase flow within the outlet header was then simulated with PHOENICS 3.2 from a time before the occurrence of flow reversal up to channel heat up, specifically, from 17000 seconds to 21010

seconds of the test. The header and its seven connecting lines of different sizes and orientations were imported to PHOENICS from AutoCAD engineering drawings (Figure 5), which include five outlet feeders, one boiler riser and one dead-ended pressure relief line. This latter pipe was expected to be important during the transient process due to its internal volume and height relative to the header, i.e. it may have had an effect on the flow field and steam distribution within the header.

The dimensions of the resultant computational domain are 0.668 m x 1.050 m x 0.675 m in the X, Y, and Z co-ordinate directions, respectively. Since this geometry involves pipe components with small diameters and degrees of inclination that require fine resolution, the non-uniform grid generation over the computational domain has led to a large number of cells, i.e., 42 x 59 x 43 in the X, Y, and Z directions, respectively. As a result of this, and the fact that almost negligible velocity magnitude exists in the dead-ended pipe, considerable

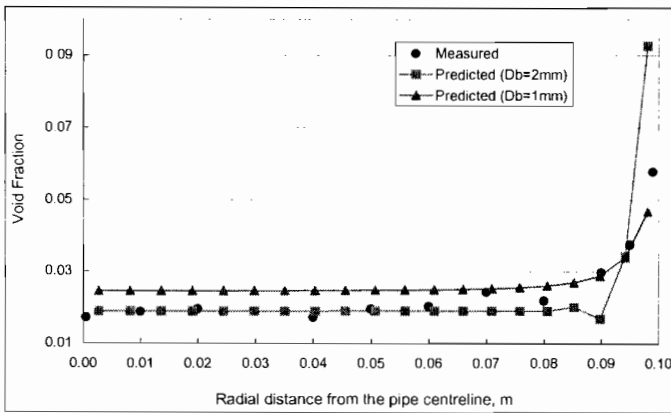


Figure 1. Wall void peaking under bubbly flow conditions ( $J_g = 0.033$  m/s)

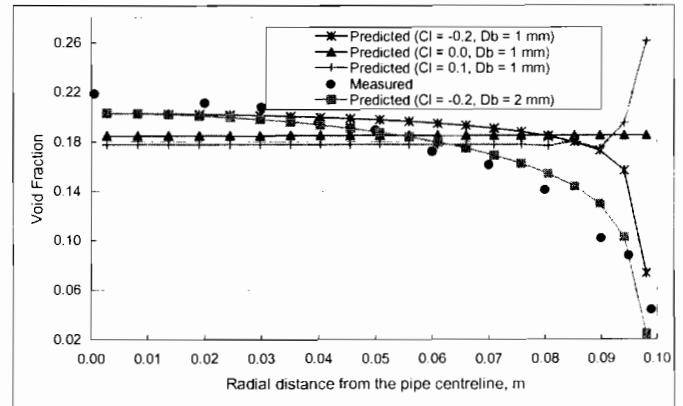


Figure 3. Core void peaking under churn bubbly flow conditions ( $J_g = 0.26$  m/s)

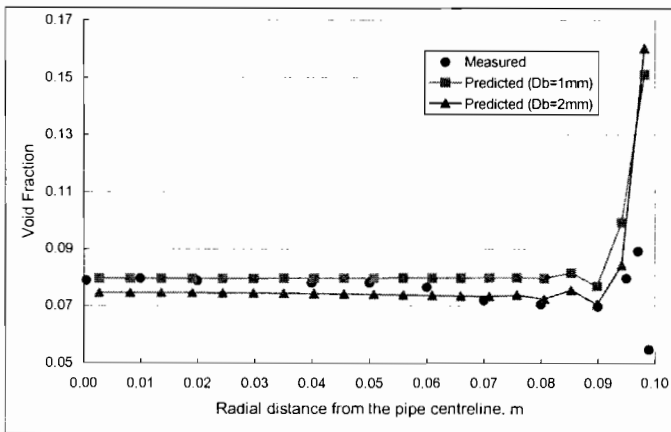


Figure 2. Wall void peaking for a higher void fraction ( $J_g = 0.11$  m/s)

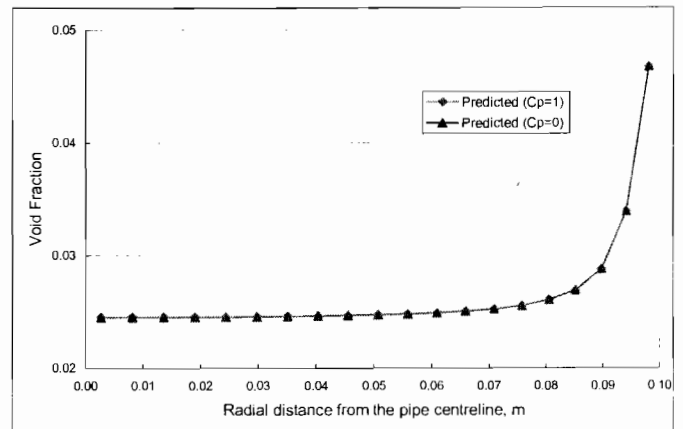


Figure 4. Effect of interfacial pressure force ( $C_p$ ) on wall void peaking ( $J_g = 0.033$  m/s)

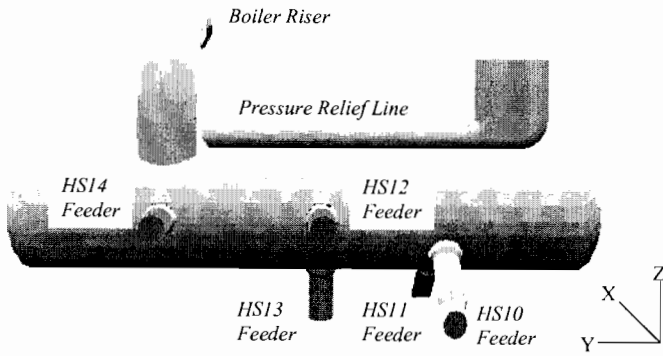


Figure 5. The outlet header geometry showing connecting lines

CPU time was required for the convergence of even one transient simulation step.

#### DETAILS OF THE MODEL

The interfacial drag was considered as the source for inter-phase momentum transfer. For phase  $i$  momentum equations, the drag force per unit volume is (CHAM 1999b)

$$F_D = C\rho_i\alpha_i\text{MAX}(\alpha_g, \alpha_{Low})(\phi_j - \phi_i) \quad (5)$$

where subscript  $j$  represents the other phase in the mixture, and  $\alpha_{Low}$  is a small positive number (1.0E-6) used to prevent the interfacial friction from vanishing numerically when the volume fraction of gas phase approaches zero. This has reasonable consequences when friction is concerned, as it ensures that very small bubbles travel at the same velocity as the carrying liquid. The value of the constant  $C$  is problem-specific, and was initially assumed to have a value of 100 1/s for the work reported herein. Equation (5) assumes that liquid water is always present in the system and has a finite volume fraction.

While the transient pressure at the exit of the boiler riser was deduced from measurements, the boundary conditions at the feeder pipes were taken from a previous 1D simulation, due to the unavailability of measurements at these locations. Before flow reversal in HS11 and HS12, at around 17100 seconds, the boundary conditions at all five feeders were set as fixed inflows where phase velocities and void were used. After the flow reversal, the

feeders from HS11 and HS12 become two additional exits from the header, thus fixed pressures were also set at these outlets.

The issue of consistency then arose among the three outlet pressures, since they were obtained from different sources, with specific uncertainties and with superimposed high frequency noise. To achieve consistency such that the outflows from the three outlets during flow reversal are comparable with the measurements, two measures were adopted. The first was to denoise the measurement-derived pressure at the riser outlet, and the pressure, void and phase velocities at the feeders that were predicted with the 1D program, using a wavelet-denoising technique (ANSL 1999, Lina and Mayrand 1995). Then a steady-state validation case at 18200 seconds was run, at which time the thermosiphoning system was relatively stable with flow reversed in HS11 and HS12. Uncertainties in pressure were analyzed and applied to the pressures at the riser and HS11 feeder outlets, and the predicted outflows from the header via feeders HS11 and HS12 compared reasonably well with the measurements. These same pressure uncertainties were applied during the ensuing transient simulation.

Also, from this validation case, the predicted pressure difference across the riser pipe was found to be only about 6% different from the measurement at this time. This implies that the chosen value for the constant  $C$  in Equation (5) is reasonable, since the interfacial drag, together with buoyancy, acting on the steam phase, will determine the mixing of the two phases within the system, and eventually the pressure distribution.

#### RESULTS AND DISCUSSION

The transient simulation, launched from an initial field solved at 17000 seconds, was divided into three time periods. The first stage, covering the time period 17000 seconds to 17124 seconds, examined in detail the header flow conditions around the occurrence of the flow reversal. The second stage covered a transition period from 17124 seconds to 20724 seconds prior to flow stalling in HS11. This was designed to check for any fluid refilling from the dead-end pipe into the outlet header during this relatively long period, and to obtain an initial field for the next simulation period. The third stage focused on the flow conditions within the header around the flow stalling in HS11 from 20724 seconds to 21010 seconds. The computational time steps used for the first,

second, and third simulation periods were 4 seconds, 600 seconds, and 26 seconds, respectively. Time step independence of the predicted results was tested for the second simulation period. These time steps were selected to adequately capture the variations of the boundary conditions, and in the meantime, to reduce CPU time requirement.

Figures 6 and 7 compare the predicted flow rates during flow reversal at HS11 and HS12 with the measurements, respectively, where “6 Step” and “3 Step” indicate the number of time steps used to cover the transition period from 17124 to 20724 seconds for the time-step independence test. The measurement bands confine the experimental flow rates for almost the entire flow reversal period simulated in this work, except at the beginning when the flows start to reverse, and near the end when the flow in HS11 is stalling. There are two short duration spikes in the predicted HS12 outflow at the beginning, but they will have a negligible effect on the general conservation of the outflow from the header during the much longer flow reversal period afterwards.

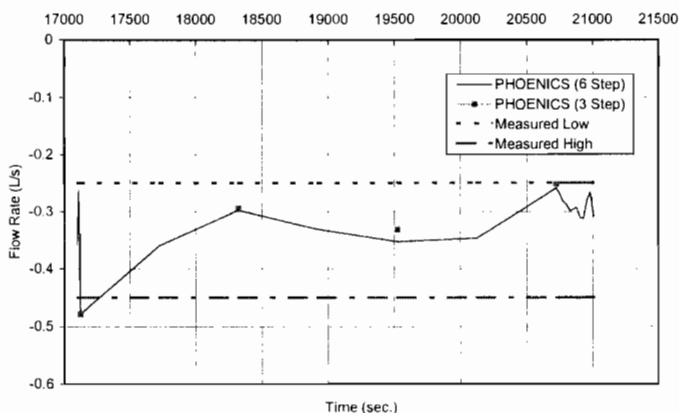


Figure 6. Comparison of flow rates at HS11

Two-phase stratification within the outlet header exists throughout the transient simulation. As observed in Figure 8, the average void within the header rapidly dropped from ~21% at 17044 seconds to ~4% at 17076 seconds, and remained at that low level until after the first flow reversal around 17096 seconds. It then increased to about 25%, and stayed there from about 18000 – 20500 seconds before the electrical fuel element simulator (FES) in HS11 started to heat up at around 20900 seconds.

The low average void before flow reversal was due to low incoming velocity and void from the outlet feeders, especially from those of HS10, HS11, and HS12. This led to high liquid levels at the outlet feeder ports for HS11 and HS12, as shown in Figure 9 at 17076 seconds for HS12 (with R2 representing the void). This may have further reduced the incoming flows from HS11 and HS12 and accelerated the occurrence of the flow reversal. The long-lasting high average void prior to HS11 heat-up was, on one hand, due to the sustained drain of the liquid during flow reversal from the HS11 and HS12 outlet feeders, as predictions indicate that the void in the outflows was extremely low. On the other hand, the incoming velocity and void from the outlet feeders of HS10, HS13, and HS14 were high during this period, namely, around 0.6 for void, and between 1 ~ 2 m/s and 2 ~ 3 m/s for liquid and steam velocities, respectively.

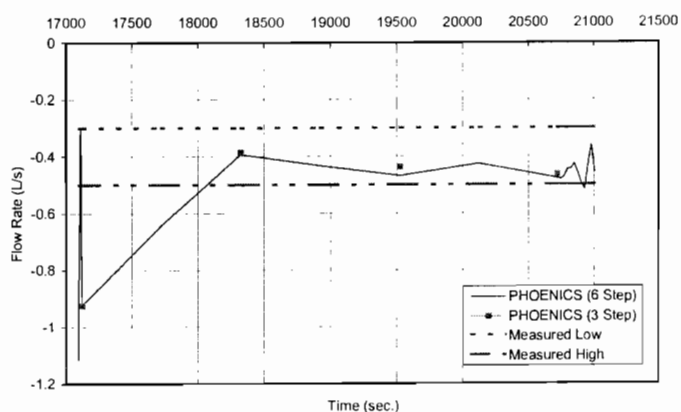


Figure 7. Comparison of flow rates at HS12

There is one concern regarding the positions of the outlet feeder ports within the header. The incoming flows from HS10 and HS11 directly impinge with each other, as do the streams from HS12 and HS13. Since the ports for HS10 and HS11 and for HS12 and HS13 are within the same plane, respectively, along the header axial direction, the jets with higher momentum (sometimes from HS11 and HS13) will deflect their low momentum counterparts. The incoming jet impingement before flow reversal could have facilitated the occurrence of flow reversal. The incoming jet momentum from HS10 before flow stalling, when the liquid level at HS11 port is relatively low, induced a circular flow pattern around HS11 port as depicted in Figure 10. In this situation, it is entirely possible for small bubbles to be entrained down into the

HS11 feeder. Accumulation of the void trapped in the HS11 feeder due to the buoyancy effect as well as pipe geometry (i.e. top horizontal section) and trace heating might then have promoted flow stalling.

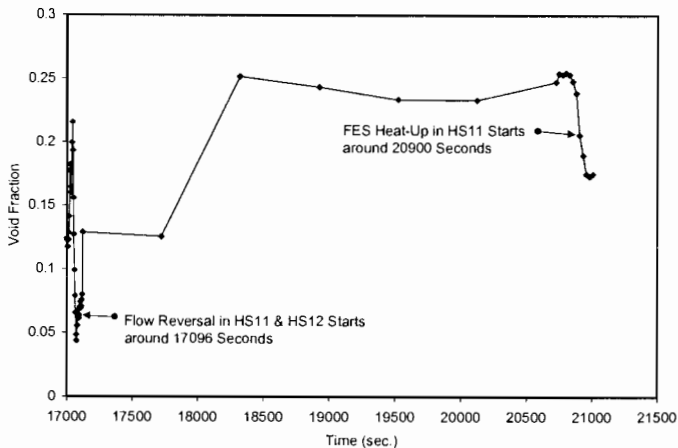


Figure 8. Predicted averaged void within the outlet header #5

There is also a concern about the distribution of the coolant among the outlet feeders. In contrast to an actual reactor, there are only five outlets feeding into the outlet header in the present geometry. Due to occasional system instability during thermosyphoning, flows can come in from HS13 and HS14 at very high velocity. Figure 11 shows that at 17124 seconds, a jet with very high momentum from HS13 divided the long header with an inner diameter of only 19.4 cm into two parts. Since the outlet feeder ports for HS10 and HS11 are within the portion farthest from the boiler pipe, the resultant pressurization in this region could promote flow reversal. The high momentum jet from HS14, on the other hand, might not have posed significant adverse influence on the normal flow condition within the header in this case, since the spacious dead-ended pipe provided a damping effect on the high momentum, as shown in Figure 12 at 17036 seconds.

## CONCLUDING REMARKS

The PHOENICS multi-dimensional two-fluid model is capable of predicting steady-state turbulent two-phase flow characteristics of both air-water and steam-water

bubbly up-flows in large vertical pipes, including the lateral void fraction distribution data.

Under bubbly flow conditions and for different gas flow rates, the PHOENICS two-fluid model was able to predict quite well the wall void peaking caused by the lift force effect on the dispersed phase distribution. A good agreement between the predictions and the experimental data (Ohnuki et al 1997) has been shown while using the same lift force coefficient value ( $C_L = 0.1$ ). There is a significant effect of the bubble diameter,  $D_b$ , on the lateral gas distribution: the wall void peaking due to the lift force effect is greater for larger bubbles than for smaller ones.

However, the conventional lift force model with a positive lift force coefficient was not able to predict the core void peaking under churn bubbly flow. Further research is needed to develop and validate more advanced constitutive equations, in particular, the lift force implementation and the bubble size model, for the applications of two-fluid model to churn bubbly flow regimes.

Also with the PHOENICS two-fluid model, the transient two-phase flow conditions within the horizontal header around the time of the unexpected observations during a test were examined. The part these conditions played in either initiating or exacerbating the unexpected observations was assessed. This investigation, aided with flow animations across space or over time produced from Tecplot, has made it possible to isolate the importance of the header behavior in the test rig, then to make arguments as to the likelihood of similar events occurring in a full-scale facility.

The two-fluid CFD modeling could be used to simulate both steady-state and transient gas-liquid flows in large piping components, in particular, for nuclear safety assessment on either design-stage or existing utilities.

## REFERENCES

Agranat, V., Kawaji, M., Hasanein, H., Chan, A.M.C. and Yoshioka, Y., 1996, *Mathematical Modelling of Steam/Water Two-Phase Flows in Large Diameter Pipes at Elevated Pressures*, Proceedings of the Fourth Annual Conference of the CFD Society of Canada, Ottawa, Ontario, pp. 481-488.

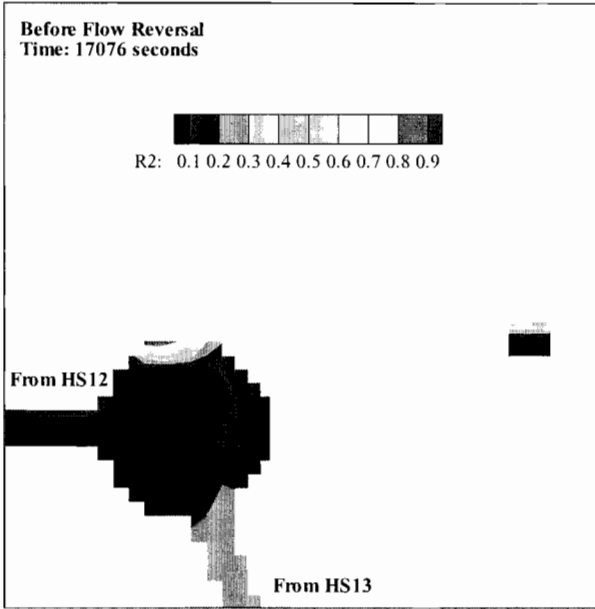


Figure 9. Void distribution at 17076 seconds across the HS12 and HS13 outlet feeder ports

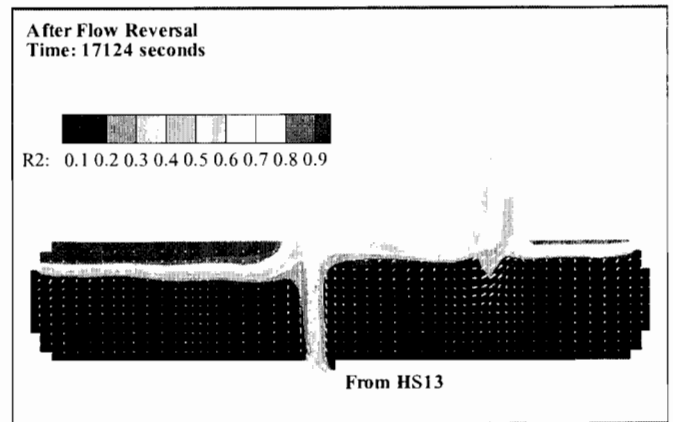


Figure 11. Void and liquid vector distribution at 17124 seconds on the mid-plane of the header

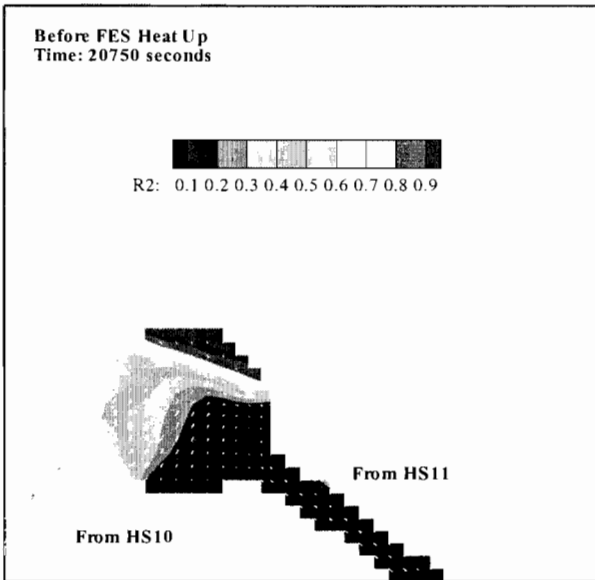


Figure 10. Void and liquid vector distribution at 20750 seconds across the HS10 and HS11 outlet feeder ports

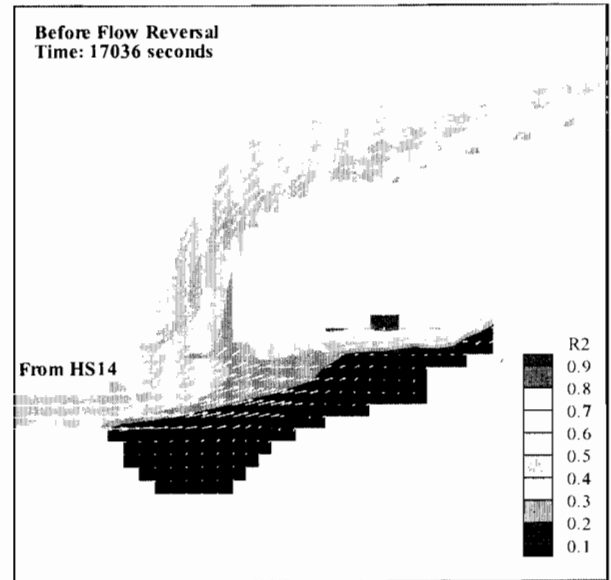


Figure 12. Void and liquid vector distribution at 17036 seconds across the HS14 outlet feeder port

Agranat, V., Kawaji, M. and Chan, A.M.C., 1998, *Modelling of Steam/Water Two-Phase Flows in Large Vertical Channels at High Pressures*, Proceedings of the Sixth Annual Conference of the CFD Society of Canada, Quebec City, Quebec, pp. XI.13-XI.18.

Alajbegovic, A., Kurul, N., Podowski, M.Z., Drew, D.A. and Lahey, R.T., Jr., 1996, *A CFD Analysis of Multidimensional Phenomena in Two-Phase Flow Using a Two-Fluid Model*, ANS Proceedings of 1996 National Heat Transfer Conference, August 3-6, Houston, Texas, HTC-Vol. 9, pp. 387-395.

ANSL, 1999, *User's Manual for Plant Analysis Workbench (PAW) Version 2.20*, Atlantic Nuclear Services Ltd., Fredericton, NB, Canada.

CHAM, 1999a, *PHOENICS Computational Fluid Dynamics Software Version 3.2*, Concentration, Heat & Momentum Limited, London, UK.

CHAM, 1999b, *POLIS for PHOENICS Computational Fluid Dynamics Software Version 3.2*, Concentration, Heat & Momentum Limited, London, UK.

Hasanein, H.A., Chan, A.M.C., Kawaji, M. and Yoshioka, Y., 1996, *Steam-Water Two-Phase Flow in Large Diameter Vertical Piping at High Pressures and Temperatures*, Proceedings of the ASME/JSME 4th International Conference On Nuclear Engineering (ICONE-4), New Orleans, Louisiana, Vol. 1- Part B, pp. 675-685.

Lahey, R.T., Jr., Lopez de Bertodano, M. and Jones, O.C., Jr., 1993, *Phase distribution in complex geometry conduits*, Nuclear Engineering and Design, Vol. 141, pp. 177-201.

Lina, J.M. and Mayrand, M., 1995, *Complex Daubechies Wavelets*, Applied and Computational Harmonic Analysis, Vol. 2, p. 219.

Ohnuki, A., Kamo, H. and Akimoto, H., 1997, *Developed Flow Pattern and Phase Distribution under Gas-Liquid Two-Phase Flow in a Large Vertical Pipe and Prediction of Phase Distribution by Multidimensional Two-Fluid Model*, Proceedings of the Eighth International Topical Meeting on Nuclear Reactor Thermal-Hydraulics, Kyoto, Japan, Vol.3, pp. 1670-1676.

Ohnuki, A., Kamo, H. and Akimoto, H., 1996, *Prediction of Developing Bubbly Flow along a Large Vertical Pipe by Multidimensional Two-Fluid Model (Development of Multidimensional Two-Fluid Model Code and Analysis under a Low Velocity)*, Proceedings of The Japan-U.S. Seminar on Two-Phase Flow Dynamics, Fukuoka, Japan, pp. 75-82.

Podowski, M.Z., 1997, *Toward Next Generation Multiphase Models of Nuclear Thermal-Hydraulics*, Proceedings of the Eighth International Topical Meeting on Nuclear Reactor Thermal-Hydraulics, Kyoto, Japan, Vol.1, pp. 53-68.